Electrochimica Acta 427 (2022) 140853

Contents lists available at ScienceDirect

Electrochimica Acta

journal homepage: www.journals.elsevier.com/electrochimica-acta

Theoretical inspection of TM-P4C single-atom electrocatalysts: High performance for oxygen reduction and evolution reactions

Chaohong Guan [a], Runxin Ouyang [a], Hong Zhu [a], Yangyang Xie [b,*]

[a] University of Michigan–Shanghai Jiao Tong University Joint Institute, Shanghai Jiao Tong University, Shanghai 200240, China
[b] School of Metallurgy and Environment, Engineering Research Center of the Ministry of Education for Advanced Battery Materials, Hunan Provincial Key Laboratory of Nonferrous Value-Added Metallurgy, Central South University, Changsha 410083, China

ARTICLE INFO

Keywords:
Oxygen evolution reaction
Oxygen reduction reaction
TMP4
Density functional theory

ABSTRACT

Developing the cost-effective or even bifunctional electrocatalysts for both oxygen evolution reaction (OER) and oxygen reduction reaction (ORR) with industrially relevant activity is highly desired for metal-air batteries at the current stage. Herein, in this work, the catalytic performances of the single transition metal (TM) atom embeds graphene sheet with the tetra-coordinates Phosphorus (TMP4) for ORR and OER are investigated based on the density functional theory method. The results demonstrate that the most promising ORR and OER catalytic activity can be achieved on the CoP4 with the smallest potential gap ΔE and the lowest overpotential of 0.37 and 0.32 eV among all TMP4 systems, respectively, and the catalytic activity is even better than that of the traditional Pt and IrO_2 catalysts. Furthermore, the AIMD and phonon dispersion calculations are conducted to confirm the thermodynamics and dynamics stability of CoP4. This work screens out promising candidates for novel graphene-based bifunctional ORR and OER catalysts and offers detailed microscopic insights into the mechanism of OER/ORR, provides a theoretical guidance for the development of further single-atom catalysts.

1. Introduction

At present, the continuously growing environmental pollution and energy depletion greatly inspire the development of renewable energy technologies including Li-ion batteries [1], fuel cells [2] and metal-air batteries [3], etc., which have emerged as systems of commercial and notable scientific interests. Among them, the rechargeable metal-air batteries [4,5] have obtained the increasing concerns due to the features in environment, cost and particularly in the potential application to replace the traditional Li-ion batteries which theoretical capacity is largely limited by the electrode materials (to date, the theoretical capacity has nearly reached) [6]. Typically, owing to the use of organic and aqueous electrolytes the metal-air batteries are divided into two groups, like Li-air batteries and Zn-air batteries, respectively. The former still needs breakthroughs in the issue of reaction products block subsequent reactions [7]; the latter is regarded as the safer and more reliable system, whose electrochemical reaction rate largely relies on the electrocatalytic processes of oxygen reduction reaction (ORR) and oxygen evolution reaction (OER) at cathodes [8,9]. Previous studies [10,11] have symbolized Pt-based catalysts are the most efficient for the ORR process, while the Ir- or Ru-based catalysts, for the OER, show promising catalytic activity. However, the mentioned catalysts before contains the noble metals so that the expensive cost is a fundamental obstacle for their large-scale practical application [12]. In this scenario, developing the cost-effective or even bifunctional electrocatalysts for both ORR and OER with industrially relevant activity is highly desired for metal-air batteries at the current stage.

Recently, two-dimensional transition metal (TM) single atom catalysts (SACs) for metal-air batteries have received tremendous attention attributed to the low cost, high specific surface area, unique chemical and physical characteristics [13], such as transition-metal disulfide dichalcogenides [14], two-dimensional (2D) metal-organic frameworks [15], etc. And intensive efforts have been made to explore/improve their ORR or OER activity and inspiring achievements have been made in recent years [16,17]. For instance, Li and colleagues [14] demonstrated the Cu-doped MoS2 exhibits the best ORR performance by theoretical screening the TM doped-MoS2 surfaces. Deng et al. [18] comprehensive studied the catalytic activity of 2D transition metal based tetracyanoquinodimethane (TM-TCNQ) monolayers and indicated that the OER activity of Ni-TCNQ is better than Fe-TCNQ, which is regarded as the most promising candidate. Also, as the most popular carbon-based 2D materials, graphene, has shown desired bifunctional catalytic activity

* Corresponding author.
E-mail address: yangyangxie2019@163.com (Y. Xie).

https://doi.org/10.1016/j.electacta.2022.140853
Received 10 May 2022; Received in revised form 8 July 2022; Accepted 12 July 2022
Available online 13 July 2022

for both ORR and OER when a TM atom was loaded on the surface [19–22]. Specifically, TM-N-C systems derived from graphene have been designed theoretically and experimentally to be one of the most favorable catalytic materials, the single TM atom coordinated with N atoms is regarded as the active center and promotes the high catalytic activity [23–26]. For the theoretical researches of TM-N-C system, the first principle based on the density functional theory (DFT) is typically adopted to screen and explore the materials with high catalytic performance [27–29]. For example, simulations indicated CoN4-gra system has been developed to have a stronger active with the overpotential of 0.69, 0.47 eV for ORE and ORR than CoN_X-gra (x=1-3) systems, exhibiting the comparably activity with the noble metal catalysts [30]. The FeN4-gra also shows more promising ORR activity than FeN_X-gra systems [31]. Lu et al. [32] theoretically proposed the MnN4-gra system and suggested its ORR activity is prior than FeN4-gra. And the catalytic mechanisms of other TM atoms embedded graphene with N coordination, such as Zn [33], Cu [34], Ni [35], have also been explored in recent years. In the experimental aspect, many TM-N-C catalysts (TM including Fe, Ni, Zn, Co, etc.) [36–38] have been practically synthesized and also exhibit promise ORR/OER activity. As Sun et al. [39] developed a highly active Cu-N-C catalyst through the pyrolysis of $Cu(NO_3)_2{\cdot}3H_2O$ and urea, showing an excellent ORR activity (5.36 mA cm^{-2} at 0.9V; $E_{1/2}$ = 0.898V vs RHE). Therefore, these results indicate that the kind of structure of TM-N-C system offers a great opportunity for the practical application of ideal ORR/OER catalysts, and the design of novel catalysts with higher activity and stability need to be challenged continuously.

As shown in periodic table, phosphorus (P) occupies the same group with N element and possesses the comparable properties. Further, P-doped carbon materials with the prospect of high catalytic activity are of thrive interests owing to the lower electronegativity and longer covalent radius than N-doped carbon, which illustrates that P doping facilitates the structural and active modification of carbon. So far, experiment results have proved P-doped structures with different carbon, including graphene [40], mesoporous carbon [41] and graphite layers [42], etc., possess the improved ORR activity. However, few works have been conducted on the catalytic performance for P and metal atoms co-doped carbon materials. Yang et al. [43] synthesized the Co and P co-operated mesoporous carbon and demonstrated its ORR activity is superior to the carbon with Co-doping or P-doping. Subsequently, they developed the P and iron co-doped carbon but the ORR activity is lower than that of Co and P co-doped carbon [44]. The P and Fe-functionalized graphene prepared by Razmjooei and co-workers exhibits a high comparable ORR activity to commercial Pt-based catalysts [45]. In addition, theoretical studies also reveal that TM-P-C (TM = Fe, Co, Ni) is a novel promising catalyst for CO oxidation with the determined catalytic energy barriers of 0.87, 0.81 and 0.79 eV, respectively [46].

To our best knowledge, few studies have been reported to comprehensively explore the bifunctional ORR/OER activity of transition metal and P co-doped graphene-based catalysts with the determined TM-P coordination numbers (TM-P4-C) to date. There is a large gray area exists in evaluating the feasibility and revealing the detailed catalytic mechanism of TM-P4-C on ORR or OER, the more appropriate TM atom for catalytic processes and the origin of the ORR/OER activities remain unclear. Herein, to breakthrough these obstacles, we introduced single TM atom (from Ti to Au) with the coordination of P into the graphene sheet as the SACs, pioneeringly and comprehensively studied its bifunctional ORR and ORE activity by first-principles calculation.

2. Experimental section

Spin-polarized first-principle calculations were implemented by Vienna ab initio simulation package (VASP) [47] with an energy cutoff of 500 eV, the Perdew-Burke-Ernzerhof (PBE) functional within the generalized gradient approximation (GGA) was adopted to address the exchange-correlation interactions [48,49]. The P and TM doped 5 × 5 × 1 graphenes were modeled with a vacuum thickness of 15Å and optimized with a Γ centered 2 × 2 × 1 k-point sampling, specially, the 5 × 5 × 1 k-point was employed to calculate the density of states (DOS). During the optimized process, all atoms were relaxed until the convergence criterions of energy (1 × 10-6 eV) and force (0.02 eV $Å^{-1}$) are reached. DFT-D3 developed by Grimme was utilized for the van der Waals correction [50]. The implicit solvent model was employed to consider the solvation effect by VASPsol program under the water conditions [51]. In addition, AIMD simulations were carried out to explore the thermodynamic stability of TM-P4-C catalysts at. The Phonopy was adopted to calculate the harmonic phonon dispersion, detailed information can be found in supporting information.

The Gibbs free energy changes (ΔG) of oxygen-containing reaction intermediates on TM-P4-C are defined as [52]:

$$\Delta G = \Delta E + \Delta ZEP - T\Delta S + \Delta U$$

Where ΔE is the energy calculated by density functional theory (DFT) method, *ZEP* and S are the zero-point energy and entropy, respectively, which can be obtained by the frequency analysis through VASPKIT package [53] (summarized in Table S1) . T is set as the room temperature of 298.15 K. In addition, the influence of applied electrode potential is considered by the term of Δ*U*.

Binding energies of TM-P4-C will be confirmed by the E_b as shown in following [54]:

$$E_b = (E_{TM-P4-C} - E_{P4-C} - E_{TM})$$

in which $E_{TM-P4-C}$ is the total energy of TM atom with the coordination of P embedded into graphene sheet, E_{P4-C} and E_{TM} represent the energy of P4-C and TM atom, respectively. In addition, according to previous studies [55–56], the formation energies were calculated to assess the formation possibility and stability of these catalysts. And the adsorption free energy of reaction intermediates on TM-P4-C surfaces was determined by [52]

$$\Delta E_{ads} = E_{O^*/OH^*/OOH^*} - E_* - E_{O/OH/OOH}$$

$$E_O = E_{H_2O} - E_{H_2}$$

$$E_{OH} = E_{H_2O} - 1/2E_{H_2}$$

$$E_{OOH} = 2E_{H_2O} - 3/2E_{H_2}$$

where $E_{O^*/OH^*/OOH^*}$ and E_* represent the total energy of TM-P4-C with and without the adsorption of oxygen-containing groups, $E_{O/OH/OOH}$ can be calculated according to the energies of H_2O and H_2 molecules.

3. Results and discussion

3.1. Stability of TM-P4-C catalysts

Recently, TM and P co-doped carbon SACs have caught extensive attentions due to the similar properties with N and exhibit the resembled configurations with TM-N4-C systems, as displayed in Fig. 1a, the single TM atom embeds graphene sheet with the tetra-coordinates P (TMP4). Via DFT calculations, for the final optimized structures (the corresponding stable configurations are illustrated in Fig. S1), the details of binding energies (E_b), formation energies and TM-P bond lengths are listed in Table S2, the negative values of E_b certify the stability of TMP4. Meanwhile, the bader charge analysis was conducted to evaluate the strong interactions between P4-C and TM atoms (Table S2). For the comparison of binding energies and cohesive energies, we adopted the cluster energies ($E_{clus} = E_{bind} - E_{coh}$) to evaluate the aggregation possibility of the TM atoms, E_{bind} and E_{coh} are binding energy and cohesive energy of TM atoms ($E_{coh} = \frac{E_{TM-bulk}}{N} - E_{TM-single}$), according to this definition, the criteria of E_{clus}< 0 eV should be satisfied for a

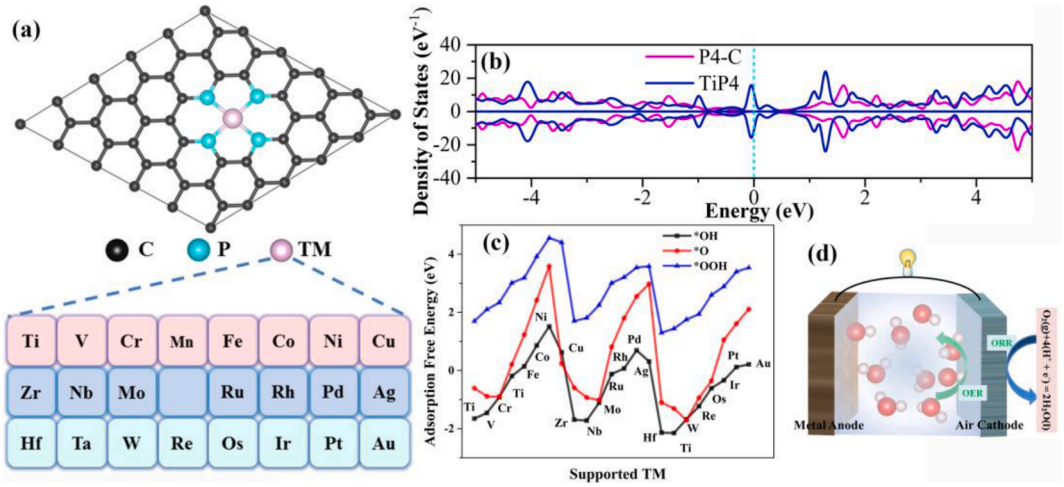

Fig. 1. (a) Top view of P4-C with a transition metal atom (from Ti to Au) doped in the center, black, blue and pink represent the carbon, phosphorus and transition metal atom, respectively. (b) Density of states (DOS) of P4-C and TiP4 with the Fermi level referred to 0 eV. (c) Comparison of adsorption free energies of related intermediates (OH, O, OOH) on TMP4. (d) Schematic model of a metal-air battery.

thermodynamically stable TMP4 structure. The detailed E_{bind}, E_{coh} and E_{clus} are listed in Table S3. Results indicate that the $E_{clus} < 0$ eV cannot be achieved for Nb, Ag, W, Os and Pt, which tend to aggregate into clusters on 4PC. And the transferred charges from TM atoms to P4-C induce to the TM atom charged positively, hence, the site of charged TM will be regarded as the adsorption and catalytic centers during the ORR/OER process. Fig. 1b depicts the DOS of P4-C and TiP4, more electronic states will be introduced to the gap near the Fermi level by the d orbitals of TM atoms when they embed to P4-C, which promotes the increased electric conductivity. And the influences of the introduced d orbitals on the ORR/OER electrocatalytic performance were discussed detailly in the section 3.3.

3.2. Bifunctional ORR/OER catalytic activities of TMP4

For the ORR/OER process, the adsorption free energies of OH* (ΔE_{OH^*}), O* (ΔE_{O^*}) and OOH* (ΔE_{OOH^*}) on catalyst surface determine the free energy of each reaction step. As a matter of common knowledge, the ideal catalyst will provide a 1.23V reaction free energy for every step of ORR/OER with no overpotential, thus, for designing the novel catalysts, the suitable adsorption free energies of intermediates should be guaranteed to maintain the low reaction overpotential. In this work, the adsorption free energies for OH*, O* and OOH* on TMP4 are compared and listed in Fig. 1c, which clearly demonstrates that the ΔE_{ads} of species containing oxygen are determined by the optimized TMP4 structures. Moreover, it can be confirmed that the TMP4 catalysts prefer to capturing hydroxide group with the relatively lower ΔE_{OH^*} ranging from -2.15 to 1.5 eV. For all intermediates adsorption on TMP4, the changes of free energy are similar with the increased TM atomic numbers (3d, 4d and 5d elements). The strongest chemical bond formed between OH and HfP4 and TaP4. For O adsorption, the lower ΔE_{O^*} are presented on the former of 3d, 4d and 5d elements embedded P4C than that of the later TM for the same period, respectively, which may induce the lower ORR activities referring to Norskov's theory [57]. In addition, the OOH group exhibits the highest adsorption free energy and the HfP4 structure has the most stability for the adsorption of OOH.

As known, the potential always deviated from the balanced potential to ensure the spontaneous reaction of ORR/OER catalytic process [58], in this work, E is defined to represent the lowest deviated potential. Typically, for ORR process, the E_{ORR} is lower than the standard potential of 1.23 V vs. RHE at 298 K, while the E_{OER} is higher than that. Moreover, previous study has reported that the potential gap ($\Delta E = E_{OER} - E_{ORR}$) is effectively suitable to present the bifunctional catalytic activity [6], and the smaller ΔE suggests the better bifunctional catalytic performance. The calculated polarization curves (describing detailly in the support information) for OER/ORR, as shown in Fig. 1a, exhibit the same principle, i.e. the smaller ΔE corresponds to the higher ORR/OER catalytic efficiency. Therefore, for us, exploring novel catalysts with the lowest ΔE is still on the road.

Fig. 2a displays the catalytic mechanisms of the ORR (blue) and OER (green) reaction process over TMP4, and the related E_{OER}, E_{ORR} and ΔE are calculated and shown in Fig. 2b. For the all TMP4 catalysts, CoP4 exhibits the best OER, ORR and bifunctional catalytic activities with $E_{OER} = 1.55\ V$, $E_{ORR} = 0.86\ V$ and $\Delta E = 0.69V$, respectively, which are better than that of Ni-SAC reported recently by Zhang and co-workers [58] ($E_{OER} = 1.62\ V$, $E_{ORR} = 0.59\ V$ and $\Delta E = 1.03V$). Followed by the PdP4 ($E_{OER} = 1.98\ V$, $E_{ORR} = 0.69\ V$ and $\Delta E = 1.29V$), RhP4 ($E_{OER} = 1.73\ V$, $E_{ORR} = 0.07\ V$ and $\Delta E = 1.66V$), PtP4 ($E_{OER} = 1.79\ V$, $E_{ORR} = 0.12\ V$ and $\Delta E = 1.67V$), AuP4 ($E_{OER} = 1.9\ V$, $E_{ORR} = 0.21\ V$ and $\Delta E = 1.69V$) and NiP4 ($E_{OER} = 2.07\ V$, $E_{ORR} = 0.36\ V$ and $\Delta E = 1.71V$). Beyond that, others show a relatively lower bifunctional catalytic activity.

To further unveil the OER/ORR catalytic performance of TMP4 systems, the change of free energy of every reaction pathway was analyzed. Typically, the OER process related to four steps, including the dissociation of H_2O to form *OH, *OH converts to *O and H^+, subsequently *O reacts with H_2O molecule to product *OOH and H^+, and following *OOH will dissociate into H^+ and O_2, the detail reaction processes are described in Support Information. Figs. 2c and S2 exhibit the free energy diagrams of every OER reaction step over TMP4 systems, containing the Gibbs free energy at U=0 and 1.23 V. The applied external voltage will promote the energy of every reaction process shifts up and down, and the free energy of each step decreases or keeps unchanged with the direction of OER/ORR reactions sequentially indicating that the spontaneous catalytic reaction can be presented. Meanwhile, the ΔG was calculated to determine the potential-limited step. Results show that the free energy differences of first step for OER (ΔG_{OH^*}) over the TMP4 systems (TM = Ti, V, Cr, Mn, Zr, Nb, Mo, Ru, Hf, Ta, W, Re, Os, Ir) are negative ranging from -2.15 to -0.12 eV, demonstrating the strong bonding interactions between TM and *OH intermediate. Therefore, the third or fourth proton-coupled electron transfer steps of *O converting to *OOH and *OOH converting to O2 fragment, respectively, and the desorption of O_2 from the TMP4 surfaces become the overpotential-limiting steps. As embedded in Fig. 2 and S2, the calculated overpotentials (η^{OER}) of TiP4 (2.0 V), VP4 (1.76 V), CrP4 (2.01 V), MnP4 (1.57 V), ZrP4 (1.99 V), NbP4 (1.88 V), MoP4 (2.03 V), RuP4 (0.97 V), HfP4 (2.39 V), TaP4 (2.25 V), WP4 (2.23 V), ReP4 (1.75 V), OsP4 (1.72 V) and IrP4 (0.80 V) indicate that the high enough input

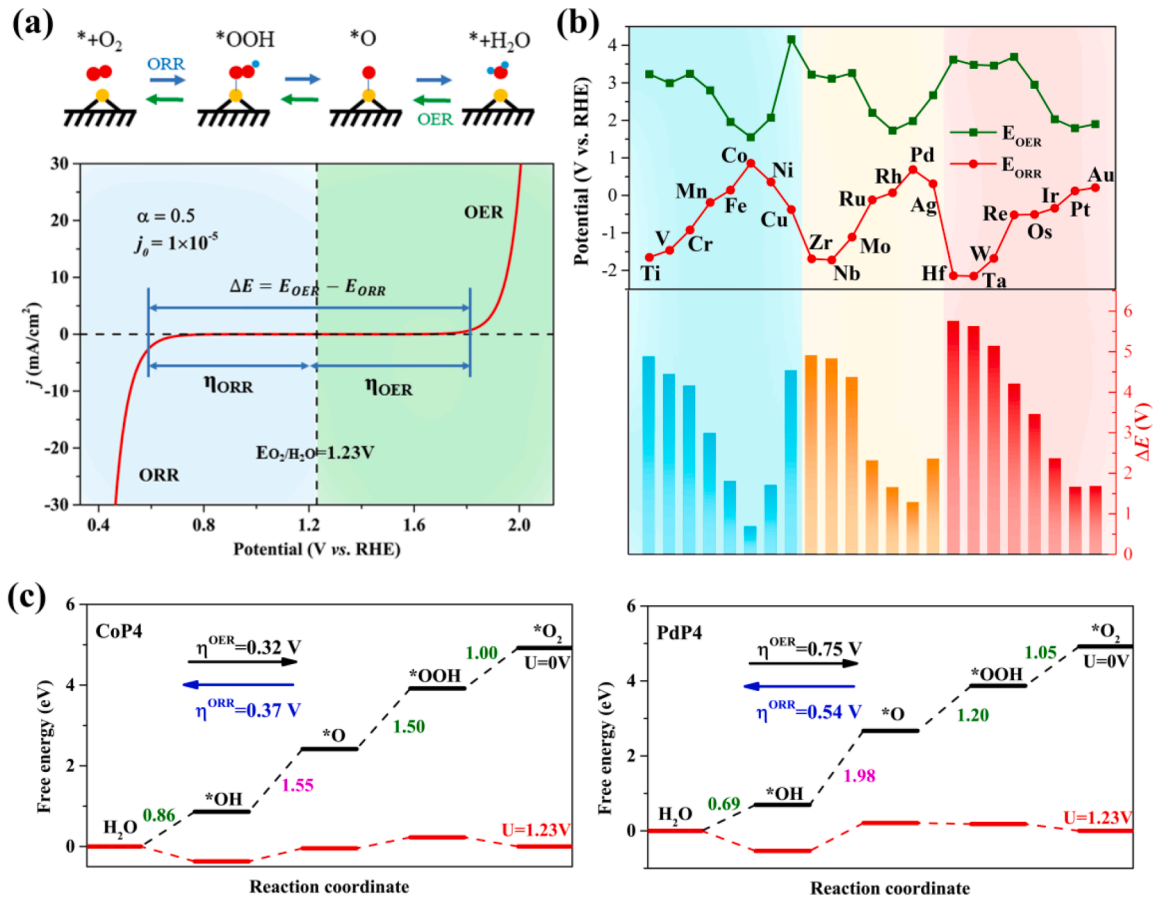

Fig. 2. (a) The pathways of ORR (blue) and OER processes, the lower figure shows the theoretical polarization curves for ORR/OER catalytic performance, the detail calculated methods are shown in supporting information. (b) The related E_{OER}, E_{ORR} and ΔE for different TM-P4 systems. (c) The calculated free energy diagrams of CoP4 and PdP4 at electrode potential of 0V and 1.23V.

energies are required for the effective OER catalytic performance. Additionally, previous study [59] has reported that the robust binding interaction and excess energy go against the elimination of related OER intermediates, impeding the active sites and poisoning the catalysts. Hence, the aforementioned TMP4 catalysts are not regarded as the available catalysts for OER. For TMP4 (TM = Fe, Co, Ni, Cu, Rh, Pd, Ag, Pt and Au) catalysts with the positive ΔG_{OH^*}, the overpotentials are relatively lower than those of the former TMP4 systems. Specially, for the NiP4, PdP4, AgP4 and AuP4 catalysts, converting from *OH to *O for the second proton-coupled electron transfer step is unlikely due to the larger free energy difference, and which can be considered as the potential-limiting step. In contrast, the potential-limiting step of OER is the third step over FeP4, CuP4 and PtP4 surfaces and the formation of *OOH from *O is rather difficult. According to η^{OER} for FeP4 (0.73 V), NiP4 (0.84 V), CuP4 (2.93 V), PdP4 (0.75 V), AgP4 (1.44 V), PtP4 (0.56 V) and AuP4 (0.67 V), these TMP4 catalysts can also be reported inappropriate for the OER. Remarkably, the CoP4 and RhP4 catalysts exhibit outstanding OER catalytic performance, with the η^{OER} of 0.32 and 0.50 V, respectively, which are better than or comparable to those of Pt1/PMA (0.49 V) [59], RuO2 (0.42 V) [60], ZnN4-edge (0.63 V) [61], and the commonly used IrO2 (0.56 V) [60] catalysts. Thus, the CoP4 and RhP4 can assist as the high active catalysts for the OER.

Further studies have been conducted to determine the specific ORR catalytic activities of TMP4 catalysts. It has known that the ORR is a reverse reaction of OER reaction, which also contains four proton-coupled electron transfer steps (see supporting information) on the TM active site. Therefore, Fig. 2c and Fig. S2 also indicate that the ΔG_{OH^*} of TMP4 (TM = Ti, V, Cr, Mn, Zr, Nb, Mo, Ru, Hf, Ta, W, Re, Os and Ir) for ORR process are positive and this step can be considered as the potential-limiting step with the much higher overpotentials. Meanwhile, the formation of H2O will be impeded by the robust interaction between OH group and TMP4 catalysts for the final step of ORR. With reference to the η^{ORR} of TiP4 (2.88 V), VP4 (2.69 V), CrP4 (2.15 V), MnP4 (1.42 V), ZrP4 (2.92 V), NbP4 (2.95 V), MoP4 (2.34 V), RuP4 (1.35 V), HfP4 (3.37 V), TaP4 (3.38 V), WP4(2.91 V), ReP4 (2.46 V), OsP4 (1.84 V) and IrP4 (1.57 V), high energy is required for these catalysts to proceed the ORR process, thus, these TMP4 catalysts can be abandoned for the ORR. In contrast, the systems with the negative ΔG_{OH^*} have the relative lower overpotentials. While, for CuP4 catalyst, the strong binding interaction blocks the formation of *OH from *O and brings a higher overpotentials. Furtherly, the values of η^{ORR} for CuP4 (1.61 V), FeP4 (1.09 V), NiP4 (0.87 V), RhP4 (1.16 V), PdP4 (0.54 V), AgP4 (0.92 V), PtP4 (1.11 V) and AuP4 (1.02 V) can not comparable to that of the metal Pt catalyst (0.45 V) [60], hence, these catalysts are also not appropriated for the ORR process. Specially, the CoP4 catalyst, with the lower ORR overpotential of 0.37 V and the step of *OH converting to H2O being the potential limiting, exhibits the superior ORR catalytic performance.

The solvent effect in a water environment is considered on the CoP4 catalyst, which exhibits the best bifunctional catalytic performance. As shown in Fig. S3, the η^{OER} value is slightly increased by 0.07 V (the OER overpotential is 0.32 V in vacuum), and the η^{ORR} value increases to 0.52 V (the ORR overpotential is 0.37 V in vacuum), which also can comparable to that of the metal Pt catalyst [60].

3.3. *Highly reactive nature of the bifunctional catalysts*

As known, finding suitable descriptors to describe the chose conformation and exploring the correlation between these descriptors

and adsorption free energies of every intermediate is an effective method to develop high performance electrocatalysts. To gain insights into the catalytic activity of TMP4 catalysts, the correlations between adsorption free energies of each intermediate containing oxygen were studied. As shown in Fig. 3a, the linear relationship is existing between the adsorption free energies of *OH (ΔG_{OH^*}), *O (ΔG_{O^*}) and *OOH (ΔG_{OOH^*}) with ΔG_{OH^*}, detailly, ΔG_{O^*} and ΔG_{OOH^*} would be expressed via equations of $\Delta G_{O^*}=1.36\Delta G_{OH^*}+1.18$, $\Delta G_{OOH^*}=0.9\Delta G_{OH^*}+3.25$, respectively, revealing a strong correlation between ΔG_{O^*} and ΔG_{OOH^*}.

In addition, the volcano-curve has been extensively reported as a forceful tool for screening and developing the electrocatalysts with the high catalytic performance [54]. As depicted in Fig. 3b, showing the η^{OER} with a descriptor of $(\Delta G_{O^*} - \Delta G_{OH^*})$ and the η^{ORR} with a descriptor of ΔG_{OH^*}, respectively. Obviously, a strong correlation can be found between η^{OER} and $(\Delta G_{O^*} - \Delta G_{OH^*})$, implying that the second proton-coupled electron transfer step is the key step for the OER over most TMP4 catalysts. Meanwhile, the strong correlation also exists between η^{ORR} and ΔG_{OH^*}, demonstrating that the desorption of *OH plays a key role in the ORR catalytic process. For the both volcanos, CoP4 catalyst occupies the top owing to the moderate adsorption interaction between TMP4 and OER/ORR intermediates, thus performing the highest activity for the OER/ORR process with the minimum η^{OER} (0.32 V) and η^{ORR} (0.37 V). Therefore, the CoP4 can be regarded as the promising bifunctional OER/ORR electrocatalyst and better than IrO2 and Pt catalysts. The optimized stable structures of reaction intermediates adsorbed on CoP4 are displayed in Fig. 3d.

Besides that, the electronic properties of all TMP4 catalysts were calculated to evaluate the reactivity and mechanism of bifunctional OER/ORR process. Figs. 4a and S3 exhibit the d-orbital DOS of the embedded TM atoms for different TMP4 systems. Previous reports [62–64] have announced that the d-band center (E_d, obtaining from d orbital of TM atom) can be extensively used to furtherly expose the catalytic properties, therefore, which is labeled in the plots of d-orbital DOS (Figs. 4a and S4). Results suggest that, in the same period, the position of E_d will move toward to a more negative value relative to Fermi level with the increased d electron numbers of TM atoms, accordingly, causing the changed adsorption strengthen of every intermediate over TMP4 catalysts. Generally, the adsorption is weaker with a more negative E_d of TM atom, which can be explained by the hybridization between TM-d orbital and the electron states of adsorption species. As displayed in Fig. 4b, the hybridization of orbitals promotes the production of antibonding and bonding states. And the antibonding states are highly occupied when the E_d is located at a more negative value, which weakens the adsorption. Moreover, the high concentrations of d free electrons near Fermi level will devote rich electrons to reaction intermediates, resulting in the strong adsorptions and challenges for produce releasing (such as TiP4 system). In constant, the low d-electrons concentrations of catalysts could not maintain the effective adsorption of reaction intermediates (AgP4). Hence, for OER/ORR process, a suitable E_d position (a modest adsorption strengthen of intermediates) plays a key role for screening catalysts. In addition, Fig. 4c and (d) show the correlations between bifunctional catalytic activity

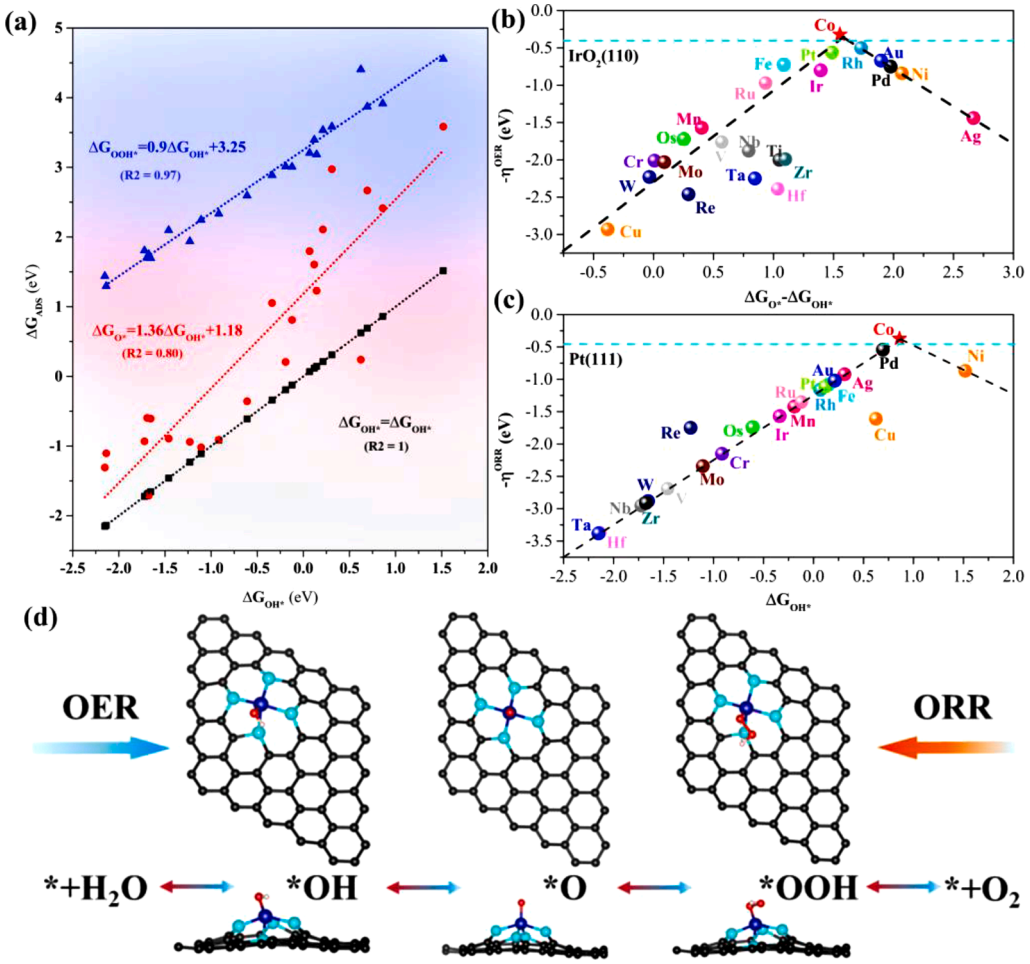

Fig. 3. (a) Calculated ΔG_{OH^*}, ΔG_{OOH^*} and ΔG_{O^*} compared with ΔG_{OH^*} for each TMP4 catalysts. Volcano curves for (b) $-\eta^{OER}$ vs. $\Delta G_{O^*} - \Delta G_{OH^*}$ and (c) $-\eta^{ORR}$ vs. ΔG_{OH^*} for different TMP4 catalysts, blue lines represent the overpotentials of IrO2(110) and Pt(111) catalysts, respectively. (d) displays the stable configurations of *OH, *OOH and *O adsorbed on CoP4.

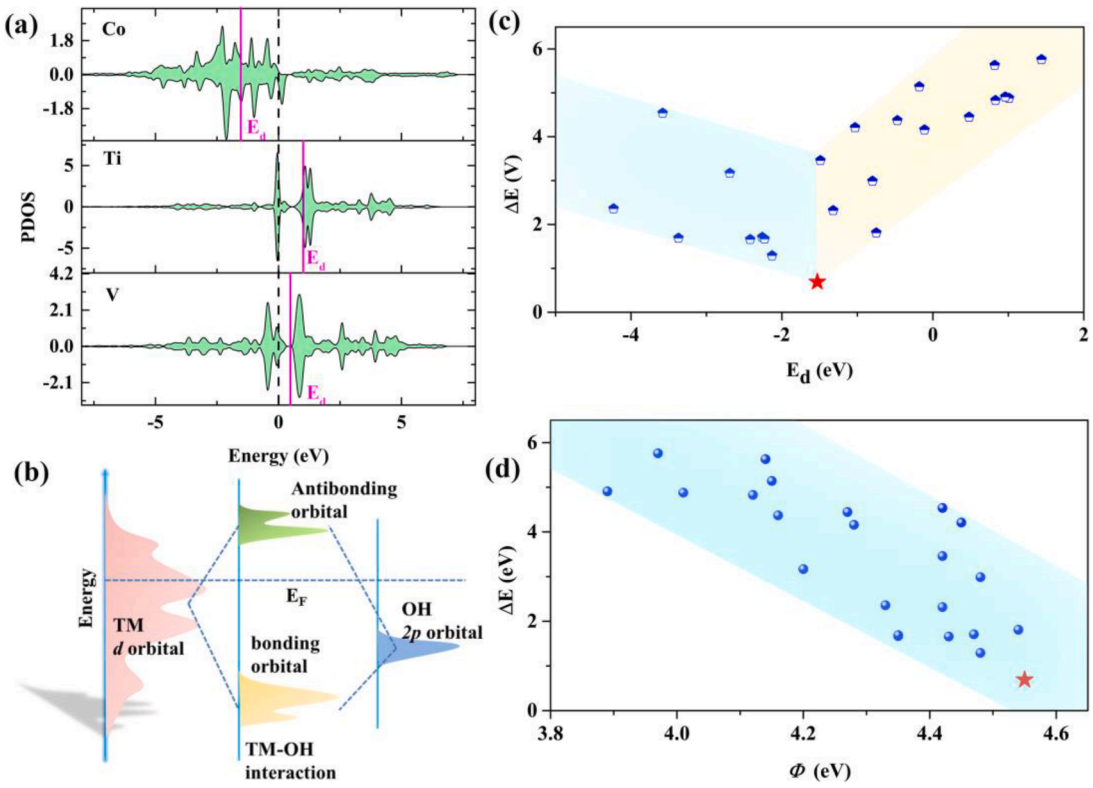

Fig. 4. (a) Partial density of states (PDOS) of d orbitals for Co, Ti and V embedded P4C systems, dotted and red lines represent the Fermi level and the d-band center (E_d) of TM atoms, respectively. (b) The schematic diagram demonstrating how TM atom interact with OH onTMP4. (c) and (d) display the correlation between E_d, work function and change in bifunctional potential ΔE for the TMP4 systems.

(ΔE) and E_d, work function (Φ, which can imply the ability of charge transfer for configuration, Table S4 displays the values of electrostatic potential (φ), E-fermi (E_F)), indicating that the closer to -1.53 V the E_d is or the larger the work function is, the better the bifunctional catalytic activity is. In summary, the CoP4 with the suitable adsorption strengthen exhibits the best bifunctional catalytic performance due to the optimized electronic structure, which is a result of the synergistic effect with a modest E_d and a large work function for Co atom. The PDOS and charge density difference [65] of intermediates adsorption (Fig. S5) on CoP4 indicate that the adsorption attributes to the charges transfer, originating from the hybridization between Co-d and p orbitals of oxygen - containing groups.

In the last, the thermodynamic stability of CoP4 catalyst is then evaluated by AIMD simulations in the NVT ensemble (300 K). As shown in Fig. 5a and b, the energy and temperature oscillate near the initial values, and the structure of CoP4 is preserved well (Fig. 5c) after 300 K dynamic simulation for 10 ps. Additionally, the mean square displacements (MSD) at 400, 500, 600 and 700 K have been calculated to further evaluate the thermodynamic stability. As shown in Fig. S6, the MSD curves at 400, 500 and 600 K maintain flatten during the simulation time, indicating that the atoms vibrate at the lattice sites to maintain the structure of CoP4. At 700 K, the MSD lightly increases at the early time, resulting in the structural distortion and the reduced stability of CoP4 (as shown in Fig. S5b). Though, the Co atom is still bonding with P atoms

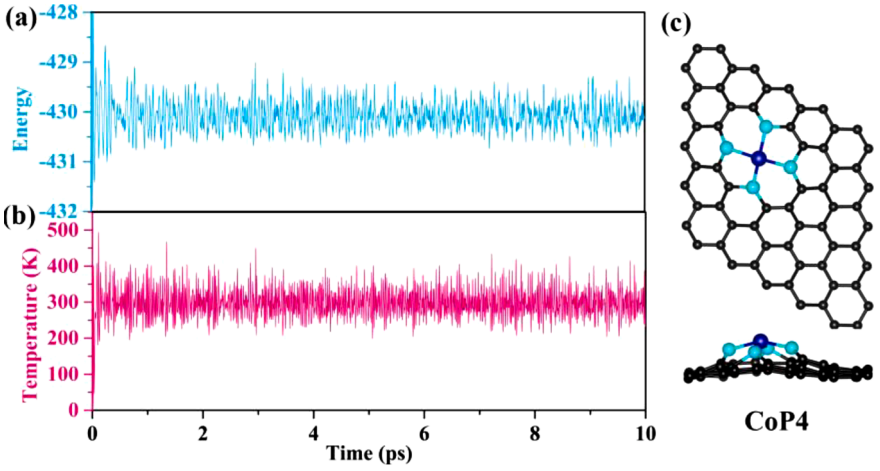

Fig. 5. (a)Total energy and (b) temperature evolution versus the time for CoP4 catalyst, and the simulation time is 10 ps at 300 K. (c) exhibits the geometric structure of CoP4 after 10 ps AIMD.

with an average bond length of 2.2 Å, which is lightly larger than that of ground-state CoP structure (2.07 Å). Therefore, it can be concluded that the CoP4 serves as an efficient bifunctional OER/ORR catalyst with high stability. From the Fig. S7, we observe stable phonon modes in this structure (without imaginary frequencies), revealing that the CoP4 is dynamically stable.

4. Conclusions

In this work, the application potential of transition metal and P co-doped graphene-based SACs (TMP4) as the bifunctional ORR/OER electrocatalysts has been comprehensively explored by using first-principle calculations. Results demonstrate that the negative binding energies between TM and P4C can guarantee the stability of the structures of TMP4. Then, the bifunctional ORR/OER activity of TMP4 were evaluated, and the CoP4 structure, whose bifunctional catalytic activity are even better than that of Pt and IrO_2 catalysts, exhibits the most promising bifunctional ORR and OER catalytic performances with the low overpotentials of 0.37 and 0.32 eV (the smallest ΔE), respectively. Based on the scaling relation between OH*, O* and OOH*, we established the volcano plots to suggest the activity tendency of ORR and OER processes on TMP4, showing that CoP4 catalyst occupies the top owing to the moderate adsorption interaction between TMP4 and OER/ORR intermediates. In addition, the PDOS, d-band center (E_d) and work function were calculated to clarify the origin of highly reactive nature of TMP4. Furthermore, the AIMD simulation was conducted to evaluate and guarantee the thermodynamic stability of CoP4 catalyst. The present results theoretically accentuate that CoP4 is a promising electrocatalyst for ORR and OER with high activity and stability.

Supporting Information

Supporting figures and tables. And the detail description of the calculation methods, including the reaction pathways of ORR and OER, the free energy change of each step, the overpotential for ORR and OER, and the measurement of polarization curves.

CRediT authorship contribution statement

Chaohong Guan: Conceptualization, Methodology, Investigation, Writing – original draft. **Runxin Ouyang:** Methodology, Data curation. **Hong Zhu:** Visualization. **Yangyang Xie:** Software, Supervision.

Declaration of Competing Interest

The authors declare that they have no known competing financial interests or personal relationships that could have appeared to influence the work reported in this paper.

Data availability

Data will be made available on request.

Acknowledgments

This work was supported by the National Natural Science Foundation of China (51602196, 52072240), the Shanghai Automotive Industry Corporation (1714), and the Materials Genome Initiative Center at Shanghai Jiao Tong University. All simulations were performed at the Shanghai Jiao Tong University High Performance Computing Center.

Supplementary materials

Supplementary material associated with this article can be found, in the online version, at doi:10.1016/j.electacta.2022.140853.

References

[1] H. Li, Z. Wang, L. Chen, X. Huang, Research on advanced materials for li-ion batteries, Adv. Mater. 21 (2009) 4593–4607.
[2] M.K. Debe, Electrocatalyst approaches and challenges for automotive fuel cells, Nature 486 (2012) 43–51.
[3] Z. Chang, X. Zhang, Introduction to metal–air batteries: theory and basic principles, 1, Wiley-VCH, Weinheim, Germany, 2018.
[4] L. Li, A. Manthiram, Long-life, high-voltage acidic Zn–air batteries, Adv. Energy Mater. 6 (2016), 1502054.
[5] J. Lee, S. Tai Kim, R. Cao, N. Choi, M. Liu, K.T. Lee, J. Cho, Metal–air batteries with high energy density: Li–air versus Zn–air, Adv. Energy Mater. 1 (2011) 34.
[6] Z. Huang, J. Wang, Y. Peng, C. Jung, A. Fisher, X. Wang, Design of efficient bifunctional oxygen reduction/evolution electrocatalyst: recent advances and perspectives, Adv. Energy Mater. 7 (2017), 1700544.
[7] L. Li, X. Zhao, A. Manthiram, A dual-electrolyte rechargeable Li-air battery with phosphate buffer catholyte, Electrochem. Commun. 14 (2012) 78.
[8] A. Kraytsberg, Y. Ein-Eli, The impact of nano-scaled materials on advanced metal–air battery systems, Nano Energy 2 (2013) 468.
[9] Y. Jiao, Y. Zheng, M. Jaroniec, S.Z. Qiao, Design of electrocatalysts for oxygen- and hydrogen-involving energy conversion reactions, Chem. Soc. Rev. 44 (2015) 2060.
[10] H.G. Sanchez Casalongue, M.L. Ng, S. Kaya, D. Friebel, H. Ogasawara, A. Nilsson, In-situ observation of surface species on iridium oxide nanoparticles during the oxygen evolution reaction, Angew. Chem. Int. Ed. 53 (2014) 7169.
[11] V. Tripkovic, Thermodynamic assessment of the oxygen reduction activity in aqueous solutions, Phys. Chem. Chem. Phys. 19 (2017) 29381.
[12] Z.W. Seh, J. Kibsgaard, C.F. Dickens, I. Chorkendorff, J.K. Nørskov, T.F. Jaramillo, Z.W. Seh, J. Kibsgaard, C.F. Dickens, I. Chorkendorff, J.K. Nørskov, T.F Jaramillo, Combining theory and experiment in electrocatalysis: insights into materials design, Science 146 (2017) eaad4998.
[13] Y. Peng, B. Lu, S. Chen, Carbon-supported single atom catalysts for electrochemical energy conversion and storage, Adv. Mater. 30 (2018), 1801995.
[14] Z. Wang, J. Zhao, Q. Cai, F. Li, Computational screening for high-activity mos2 monolayer-based catalysts for the oxygen reduction reaction via substitutional doping with transition metal, J. Mater. Chem. A 5 (2017) 9842–9851.
[15] Q. Peng, J. Zhou, J. Chen, T. Zhang, Z. Sun, Cu single atoms on Ti2CO2 as a highly efficient oxygen reduction catalyst in a proton exchange membrane fuel cell, J. Mater. Chem. A 7 (2019) 26062–26070.
[16] K. Qu, Y. Zheng, S. Dai, S.Z. Qiao, Graphene oxide-polydopamine derived N, S-codoped carbon nanosheets as superior bifunctional electrocatalysts for oxygen reduction and evolution, Nano Energy 19 (2016) 373–381.
[17] L. Qian, Z. Lu, T. Xu, X. Wu, Y. Tian, Y. Li, Z. Huo, X. Sun, X. Duan, Trinary layered double hydroxides as high-performance bifunctional materials for oxygen electrocatalysis, Adv. Energy Mater. 5 (2015), 1500245.
[18] Q.M. Deng, J. Zhao, T. Wu, G. Chen, H.A. Hansen, T. Vegge, 2D transition metal–TCNQ sheets as bifunctional single-atom catalysts for oxygen reduction and evolution reaction (ORR/OER), J. Catal. 370 (2019) 378–384.
[19] W. Ju, A. Bagger, G.-P. Hao, A.S. Varela, I. Sinev, V. Bon, B.R. Cuenya, S. Kaskel, J. Rossmeisl, P. Strasser, Understanding activity and selectivity of metal-nitrogen-doped carbon catalysts for electrochemical reduction of CO_2, Nat. Commun. 8 (2017) 944.
[20] H.J. Qiu, Y. Ito, W. Cong, Y. Tan, P. Liu, A. Hirata, T. Fujita, Z. Tang, M. Chen, Nanoporous graphene with single-atom nickel dopants: An efficient and stable catalyst for electrochemical hydrogen production, Angew. Chem. Int. Ed. 54 (2015) 14031–14035.
[21] L. Zhang, Y. Jia, G. Gao, X. Yan, N. Chen, J. Chen, M.T. Soo, B. Wood, D. Yang, A. Du, X. Yao, Graphene defects trap atomic Ni species for hydrogen and oxygen evolution reactions, Chem 4 (2018) 285–297.
[22] H. Yan, H. Cheng, H. Yi, Y. Lin, T. Yao, C. Wang, J. Li, S. Wei, J. Lu, Single-atom Pd1/Graphene catalyst achieved by atomic layer deposition: remarkable performance in selective hydrogenation of 1,3-butadiene, J. Am. Chem. Soc. 137 (2015) 10484–10487.
[23] A. Zitolo, V. Goellner, V. Armel, M.-T. Sougrati, T. Mineva, L. Stievano, E. Fonda, F. Jaouen, Identification of catalytic sites for oxygen reduction in iron- and nitrogen-doped graphene materials, Nat. Mater. 14 (2015) 937.
[24] X. Fu, N. Li, B. Ren, G. Jiang, Y. Liu, F.M. Hassan, D. Su, J. Zhu, L. Yang, Z. Bai, Z. P. Cano, A. Yu, Z. Chen, Tailoring FeN_4 sites with edge enrichment for boosted oxygen reduction performance in proton exchange membrane fuel cell, Adv. Energy Mater. 9 (11) (2019), 1803737.
[25] X. Zhang, Z. Yang, Z. Lu, W. Wang, Bifunctional CoNx embedded graphene electrocatalysts for oer and orr: a theoretical evaluation, Carbon 130 (2018) 112–119.
[26] H. Yan, Y. Lin, H. Wu, W. Zhang, Z. Sun, H. Cheng, W. Liu, C. Wang, J. Li, X. Huang, T. Yao, J. Yang, S. Wei, J. Lu, Bottom-up precise synthesis of stable platinum dimers on graphene, Nat. Commun. 8 (2017) 1070.
[27] H. Xu, D. Cheng, D. Cao, X.C. Zeng, A universal principle for a rational design of single-atom electrocatalysts, Nat. Catal. 1 (2018) 339–348.
[28] X. Guo, S. Lin, J. Gu, S. Zhang, Z. Chen, S. Huang, Simultaneously achieving high activity and selectivity toward two-electron o2 electroreduction: the power of single-atom catalysts, ACS Catal. 9 (2019) 11042–11054.
[29] S. Lin, H. Xu, Y. Wang, X.C. Zeng, Z. Chen, Directly predicting limiting potentials from easily obtainable physical properties of graphene-supported single-atom electrocatalysts by machine learning, J. Mater. Chem. A 8 (2020) 5663–5670.
[30] X Zhang, Z Yang, Z Lu, W. Wang, Bifunctional CoNx embedded graphene electrocatalysts for OER and ORR: a theoretical evaluation, Carbon 130 (2018) 112–119.

[31] Y. Li, X. Liu, L. Zheng, J. Shang, X. Wan, R. Hu, X. Guo, S. Hong, J. Shui, Preparation of Fe–N–C catalysts with FeNx (x = 1, 3, 4) active sites and comparison of their activities for the oxygen reduction reaction and performances in proton exchange membrane fuel cells, J. Mater. Chem. A 7 (2019) 26147.
[32] Z. Lu, G. Xu, C. He, T. Wang, L. Yang, Z. Yang, D. Ma, Novel catalytic activity for oxygen reduction reaction on MNN4 embedded graphene: a dispersion-corrected density functional theory study, Carbon 84 (2015) 500–508.
[33] J. Li, S. Chen, N. Yang, M. Deng, S. Ibraheem, J. Deng, J. Li, L. Li, Z. Wei, Ultrahigh-loading Zinc single-atom catalyst for highly efficient oxygen reduction in both acidic and alkaline media, Angew. Chem. Int. Ed. 58 (2019) 7035.
[34] F. Li, G.F. Han, H.J. Noh, S.J. Kim, Y. Lu, H.Y. Jeong, Z. Fu, J.B. Baek, Boosting oxygen reduction catalysis with abundant copper single atom active sites, Energy Environ. Sci. 11 (2018) 2263–2269.
[35] Z. Liang, M. Luo, M. Chen, X. Qi, J. Liu, C. Liu, S.G. Peera, T.X. Liang, Exploring the oxygen electrode Bi-functional activity of Ni–N–C-doped graphene systems with N, C co-ordination and OH ligand effects, J. Mater. Chem. A 8 (2020) 20453–20462.
[36] G. Zhang, Y. Jia, C. Zhang, X. Xiong, K. Sun, R. Chen, W. Chen, Y. Kuang, L. Zheng, H. Tang, W. Liu, J. Liu, X. Sun, F. Lin, H. Dai, A general route via formamide condensation to prepare atomically dispersed metal–nitrogen–carbon electrocatalysts for energy technologies, Energy Environ. Sci. 12 (2019) 1317–1325.
[37] Y. Lin, P. Liu, E. Velasco, G. Yao, Z. Tian, L. Zhang, L. Chen, Fabricating single-atom catalysts from chelating metal in open frameworks, Adv. Mater. 31 (2019), 1808193.
[38] Y. Mun, S. Lee, K. Kim, S. Kim, S. Lee, J.W. Han, J. Lee, Versatile strategy for tuning ORR activity of a single Fe-N4 site by controlling electron-withdrawing/donating properties of a carbon plane, J. Am. Chem. Soc. 141 (2019) 6254–6262.
[39] T. Sun, Y. Li, T. Cui, L. Xu, Y.G. Wang, W. Chen, P. Zhang, T. Zheng, X. Fu, S. Zhang, Z. Zhang, D. Wang, Y. Li, Engineering of coordination environment and multiscale structure in single-site copper catalyst for superior electrocatalytic oxygen reduction, Nano Lett. 20 (2020) 6206–6214.
[40] R. Li, Z.D. Wei, X.L. Gou, W. Xu, Phosphorus-doped graphene nanosheets as efficient metal-free oxygen reduction electrocatalysts, RSC Adv. 3 (2013) 9978.
[41] D.S. Yang, D. Bhattacharjya, S. Inamdar, J. Park, J.S. Yu, Phosphorus-doped ordered mesoporous carbons with different lengths as efficient metal-free electrocatalysts for oxygen reduction reaction in alkaline media, J. Am. Chem. Soc. 134 (2012) 16127.
[42] Z.W. Liu, F. Peng, H.J. Wang, H. Yu, W.X. Zheng, J. Yang, Phosphorus-doped graphite layers with high electrocatalytic activity for the O_2 reduction in an alkaline medium, Angew. Chem. Int. Ed. 50 (2011) 3257.
[43] J. Wu, Z.R. Yang, Z.J. Wang, Q.J. Sun, R.Z. Yang, Synthesis and electrocatalytic activity of phosphorus and Co Co-doped mesoporous carbon for oxygen reduction, Electrochem. Commun. 42 (2014) 46–49.
[44] Z. Yang, J. Wu, X. Zheng, Z. Wang, R. Yang, Enhanced catalytic activity for the oxygen reduction reaction with Co-doping of phosphorus and iron in carbon, J. Power Sources 277 (2015) 161–168.
[45] F. Razmjooei, K.P. Singh, E.J. Bae, J.S. Yu, A new class of electroactive Fe- and P-functionalized graphene for oxygen reduction, J. Mater. Chem. A 3 (2015) 11031–11039.
[46] X.Y. Xu, S. Lin, H. Xu, H.S. Guo, C.Y. Zhao, Mechanistic insights into the CO oxidation reaction catalyzed by P-coordinated metal-doped graphene: The roles of phosphorus and metal atom, Appl. Surf. Sci. 556 (2021), 149776.
[47] G. Kresse, J. Furthmüller, Efficient iterative schemes for AB initio total-energy calculations using a plane-wave basis set, Phys. Rev. B 54 (1996) 11169.
[48] J.P. Perdew, Y. Wang, Accurate and simple analytic representation of the electron-gas correlation energy, Phys. Rev. B 45 (1992) 13244.
[49] J.P. Perdew, K. Burke, M. Ernzerhof, Generalized gradient approximation made simple, Phys. Rev. Lett. 77 (1996) 3865.
[50] K. Lee, É.D. Murray, L. Kong, B.I. Lundqvist, D.C. Langreth, Higher-accuracy van der waals density functional, Phys. Rev. B 82 (2010), 081101.
[51] K. Mathew, R. Sundararaman, K. Letchworth-Weaver, T. Arias, R.G. Hennig, Implicit solvation model for density-functional study of nanocrystal surfaces and reaction pathways, J. Chem. Phys. 140 (2014), 084106.
[52] H. Niu, X.H. Wan, X. Wang, C. Shao, J. Robertson, Z.F. Zhang, Y.Z. Guo, Defect engineering in a Eu2+-doped β-Al_2O_3 structure blue phosphor and its controllable zero-thermal quenching luminescence, ACS Sustain. Chem. Eng. 9 (2021) 3590–3599.
[53] V. Wang, N. Xu, J.C. Liu, G. Tang, W.T. Geng, VASPKIT: A user-friendly interface facilitating high-throughput computing and analysis using VASP code, Comput. Phys. Commun. 267 (2021), 108033.
[54] H. Niu, Z.F. Zhang, X. Wang, X. Wan, C. Shao, Y.Z. Guo, Theoretical insights into the mechanism of selective nitrate-to-ammonia electroreduction on single-atom catalysts, Adv. Func. Mater. 31 (2021), 2008533.
[55] R.H. Lu, C.X. Quan, C.Y. Zhang, Q. He, X.B. Liao, Z.Y. Wang, Y. Zhao, Establishing a theoretical insight for penta-coordinated iron-nitrogen-carbon catalysts toward oxygen reaction, Nano Res. (2022), https://doi.org/10.1007/s12274-022-4318-2.
[56] G.F. Xiao, R.H. Lu, J.F. Liu, X.B. Liao, Z.Y. Wang, Y. Zhao, Coordination environments tune the activity of oxygen catalysis on single atom catalysts: A computational study, Nano Res 15 (2022) 3073–3081.
[57] J.K. Nørskov, J. Rossmeisl, A. Logadottir, L. L, Origin of the overpotential for oxygen reduction at a fuel-cell cathode, J. Phys. Chem. B 108 (2004) 17886.
[58] B. Wei, Z.H. Fu, D. Legut, T C Germann, S.Y. Du, H.J. Zhang, J.S. Francisco, R. F. Zhang, Rational design of highly stable and active mxene-based bifunctional ORR/OER double-atom catalysts, Adv. Mater. (2021), 2102595.
[59] S.H. Talib, Z. Lu, X. Yu, K. Ahmad, B. Bashir, Z. Yang, J. Li, Theoretical inspection of M1/PMA single-atom electrocatalyst: ultra-high performance for water splitting (HER/OER) and oxygen reduction reactions (OER), ACS Catal. 11 (2021) 8929–8941.
[60] I.C. Man, H.Y. Su, F. Calle-Vallejo, H.A. Hansen, J.I. Martínez, N.G. Inoglu, J. Kitchin, T.F. Jaramillo, J.K. Nørskov, J. Rossmeisl, Universality in oxygen evolution electrocatalysis on oxide surfaces, ChemCatChem 3 (2011) 1159–1165.
[61] Y. Li, R. Hu, X. Wan, J.X. Shang, F.H. Wang, J. Shui, Density functional theory calculation of Zn and N codoped graphene for oxygen reduction and evolution reactions, Adv. Theory Simul. 3 (2020), 2000054.
[62] C. Ling, L. Shi, Y. Ouyang, X.C. Zeng, Nanosheet supported single-metal atom bifunctional catalyst for overall water splitting, J. Wang, Nano Lett. 17 (2017) 5133–5139.
[63] Z. Fu, C. Ling, J. Wang, A $Ti_3C_2O_2$ supported single atom, trifunctional catalyst for electrochemical reactions, J. Mater. Chem. A 8 (2020) 7801–7807.
[64] X. Liao, R. Lu, L. Xia, Q. Liu, H. Wang, K. Zhao, Z. Wang, Y. Zhao, Density functional theory for electrocatalysis, Energy Environ. Mater. 5 (2022) 157–185.
[65] Z. Xu, X. Zhang, J. Qin, R. Liu, TMN4 complex embedded graphene as bifunctional electrocatalysts for high efficiency OER/ORR, J. Energy Chem. 55 (2021) 437–443.